Defective Bone Microstructure in Hydronephrotic Mice: A Histomorphometric Study in ICR/Mlac-*hydro* Mice

PANAN SUNTORNSARATOON,[1,2] KANNIKAR WONGDEE,[1,3] WACHARAPORN TIYASATKULKOVIT,[1,4] SUMATE AMPAWONG,[4] NATEETIP KRISHNAMRA,[1,2] KANCHANA KENGKOOM,[4] AND NARATTAPHOL CHAROENPHANDHU[1,2]*

[1]Center of Calcium and Bone Research (COCAB), Faculty of Science, Mahidol University, Thailand
[2]Department of Physiology, Faculty of Science, Mahidol University, Thailand
[3]Office of Academic Management, Faculty of Allied Health Sciences, Burapha University, Chonburi, Thailand
[4]National Laboratory Animal Center, Mahidol University, Thailand

ABSTRACT

Chronic renal impairment can lead to bone deterioration and abnormal bone morphology, but whether hydronephrosis is associated with bone loss remains unclear. Herein, we aimed to use computer-assisted bone histomorphometric technique to investigate microstructural bone changes in Imprinting Control Region (ICR) mice with a spontaneous mutation that was associated with bilateral nonobstructive hydronephrosis (ICR/Mlac-*hydro*). The results showed that 8-week-old ICR/Mlac-*hydro* mice manifested decreases in trabecular bone number and thickness, and an increased trabecular separation, thereby leading to a reduction in trabecular bone volume compared with the wild-type mice. Furthermore, histomorphometric parameters related to both bone resorption and formation, that is, eroded surface, osteoclast surface, and osteoblast surface, were much lower in ICR/Mlac-*hydro* mice than in the wild type. A decrease in moment of inertia was found in ICR/Mlac-*hydro* mice, indicating a decrease in bone strength. In conclusion, ICR/Mlac-*hydro* mice exhibited trabecular bone loss, presumably caused by marked decreases in both osteoblast and osteoclast activities, which together reflected abnormally low bone turnover. Thus, this mouse strain appeared to be a valuable model for studying the hydronephrosis-associated bone disease. Anat Rec, 297:208–214, 2014. © 2013 Wiley Periodicals, Inc.

Key words: bone histomorphometry; bone resorption; bone turnover; Goldner's trichrome; hydronephrosis

Grant sponsor: Mahidol University; Grant sponsor: Discovery-based Development Grant, National Science and Technology Development Agency; Grant number: P-10-11281 (to N.C.); Grant sponsor: Thailand Research Fund, the Office of the Higher Education Commission, the Faculty of Allied Health Sciences, Burapha University; Grant number: MRG5480230 (to K.W.); Grant sponsor: Royal Golden Jubilee Ph.D. Program, Thailand Research Fund–Mahidol University; Grant number: PHD/0172/2552 (to P.S.).

*Correspondence to: N. Charoenphandhu, Department of Physiology, Faculty of Science, Mahidol University, Rama VI Road, Bangkok 10400, Thailand. Fax: +66-2-354-7154.
E-mail: naratt@narattsys.com

Received 18 June 2013; Accepted 16 October 2013.
DOI 10.1002/ar.22836
Published online 14 November 2013 in Wiley Online Library (wileyonlinelibrary.com).

INTRODUCTION

Hydronephrosis is characterized by unilateral or bilateral dilation of the renal pelvis and/or renal calyces associated with gradual atrophy of the renal parenchyma due to physical or functional obstruction of the urine outflow (Toiviainen-Salo et al., 2004; Alpers, 2010). It may result from congenital malformation, calculi, inflammation, or the presence of tumors (Alpers, 2010). The affected kidney becomes slightly to massively enlarged, depending on the duration and degree of the pelvicalyceal obstruction (Alpers, 2010). Unilateral hydronephrosis can remain silent for a long period, but bilateral hydronephrosis eventually renders clinical features of polyuria and abnormal urinary electrolyte concentrations (Chandar et al., 1996; Alpers, 2010).

Little is known regarding possibility of impaired bone metabolism in hydronephrotic individuals. As chronic renal impairment often leads to a number of metabolic disturbances, such as chronic metabolic acidosis and low production of 1,25-dihydroxyvitamin D_3 [$1,25(OH)_2D_3$], both of which can profoundly affect bone metabolism (Arnett, 2003; Brandao-Burch et al., 2005; Wesseling et al., 2008), a change in bone turnover was anticipated in hydronephrosis. In this study, we investigated the microstructural changes in the trabecular bone of Imprinting Control Region (ICR) mice with a spontaneous mutation associated with bilateral nonobstructive hydronephrosis—a model named ICR/Mlac-*hydro* (Ampawong et al., 2012; Kengkoom et al., 2012). This mutant strain had neither interstitial fibrosis nor glomerulosclerosis, but the kidney had a reduced expression of aquaporin (AQP)-1, AQP2, and AQP4 as compared to the wild-type littermates (Ampawong et al., 2012). Although the ICR/Mlac-*hydro* mice manifested conspicuous renal enlargement, they appeared to have normal growth rate with the body weight of young adult mutant mice being comparable with that of the wild-type littermates (Ampawong et al., 2012). As adaptive change in bone microstructure often occurs in response to changes in body weight (Faje and Klibanski, 2012), the ICR/Mlac-*hydro* mouse with normal body weight should be a suitable animal model for studying hydronephrosis-associated alteration in bone turnover.

Therefore, the principal objectives of our study were (*i*) to demonstrate whether abnormal bone turnover occurred in hydronephrotic mice; and (*ii*) to investigate the microstructural bone changes in hydronephrotic mice using bone histomorphometric technique.

MATERIALS AND METHODS

Animals

Male wild-type and ICR/Mlac-*hydro* mice (ICR mouse strain; 8 weeks old) were provided by the National Laboratory Animal Center (NLAC), Mahidol University, Nakhon Pathom, Thailand. Their biological data, including phenotype, blood profile, and renal pathology, have been reported previously (Ampawong et al., 2012; Kengkoom et al., 2012). Mice were housed in low barrier system with bedding of autoclaved wood shaving, and fed pasteurized standard chow containing 1.0% wt/wt calcium, 0.9% wt/wt phosphorus, and 4,000 IU/kg vitamin D (CP, Bangkok, Thailand), and 7–10 ppm chlorinated water *ad libitum* under 12 h/12 h light/dark cycle. Room temperature was controlled at $22 \pm 2^{\circ}C$ and relative humidity was 50–60%. Their phenotype was verified before use, as described previously (Ampawong et al., 2012; Kengkoom et al., 2012). This animal study was performed in accordance with the Mahidol University policy for the care and use of animals for scientific purposes and has been approved by the institutional animal ethics committee of the NLAC.

Sample Collection

Before sample collection, the wild-type and ICR/Mlac-*hydro* mice were humanely euthanized by CO_2 inhalation. Femora and tibiae were removed and cleaned of adhering muscles and connective tissues. Bone length was measured with a vernier caliper. Histological and microstructural bone changes were determined in *ex vivo* tibiae obtained from the wild-type and ICR/Mlac-*hydro* mice by Goldner's trichrome staining and bone histomorphometry. The concentrations of blood urea nitrogen (BUN) and blood creatinine were measured by Hitachi-902 automated blood analyzer (Hitachi Science Systems, Ibaraki, Japan), while inorganic phosphate was analyzed by phosphomolybdate-based kit using a Dimension RxL analyzer (Dade Behring, Marburg, Germany). Plasma ionized calcium and serum 25-hydroxyvitamin D levels were analyzed by ion-selective electrode and chemiluminescent immunoassay (catalog no. 310600; DiaSorin Liaison, Stillwater, MN), respectively.

Bone Histomorphometry

As described previously, tibiae from wild-type and ICR/Mlac-*hydro* mice were cleaned of adhering muscles and connective tissues and were then dehydrated in 70, 95 and 100% vol/vol ethanol for 3, 3, and 2 days, respectively (Suntornsaratoon et al., 2010; Thongchote et al., 2011; Jongwattanapisan et al., 2012). Dehydrated bone specimens were then embedded in methyl methacrylate plastic at $42^{\circ}C$ for 48 h. The resin-embedded tibiae were first adjusted to obtain the same orientation, and longitudinal sections of 7-μm thickness were cut with the use of rotary microtome equipped with a tungsten carbide blade (model RM2255; Leica, Nussloch, Germany).

Thereafter, each section was mounted on a standard microscope slide, deplastinated, dehydrated, and processed for Goldner's trichrome staining (van't Hof et al., 2003). Image captures and analyses were performed under a light microscope (model BX51TRF; Olympus, Tokyo, Japan) using an objective lens 20× and the computer-assisted Osteomeasure system operated with the software version 4.1 (Osteometric Inc., Atlanta, GA). The region of interest (ROI) covered the whole trabecular region of the proximal tibial metaphysis at 1–2 mm distal to the growth plate (i.e., secondary spongiosa). The histomorphometric parameters obtained from the Goldner's trichrome-stained sections consisted of trabecular bone volume normalized by tissue volume (BV/TV, %), trabecular number (Tb.N, mm^{-1}), trabecular separation (Tb.Sp, μm), trabecular thickness (Tb.Th, μm), osteoblast surface normalized by bone surface (Ob.S/BS, %), osteoid thickness (O.Th, μm), osteoid surface (OS/BS, %), osteoclast surface (Oc.S/BS, %), and eroded surface (ES/BS, %). Osteocyte lacunar area (Ot.Lc.Ar, μm^2) of

TABLE 1. Blood chemistry of the wild-type and hydronephrotic mice.

Group	BUN (mg/dL)	Creatinine (mg/dL)	Ionized calcium (mmol/L)	Phosphate (mg/dL)
Wild-type	24.51 ± 1.90 ($n = 9$)	0.10 ± 0.05 ($n = 9$)	1.23 ± 0.03 ($n = 4$)	11.10 ± 0.61 ($n = 5$)
Hydronephrosis	24.40 ± 2.00 ($n = 9$)	0.12 ± 0.05 ($n = 9$)	1.11 ± 0.02[a] ($n = 4$)	15.38 ± 0.39[b] ($n = 5$)

[a]$P < 0.05$ compared with the wild-type group.
[b]$P < 0.001$ compared with the wild-type group.

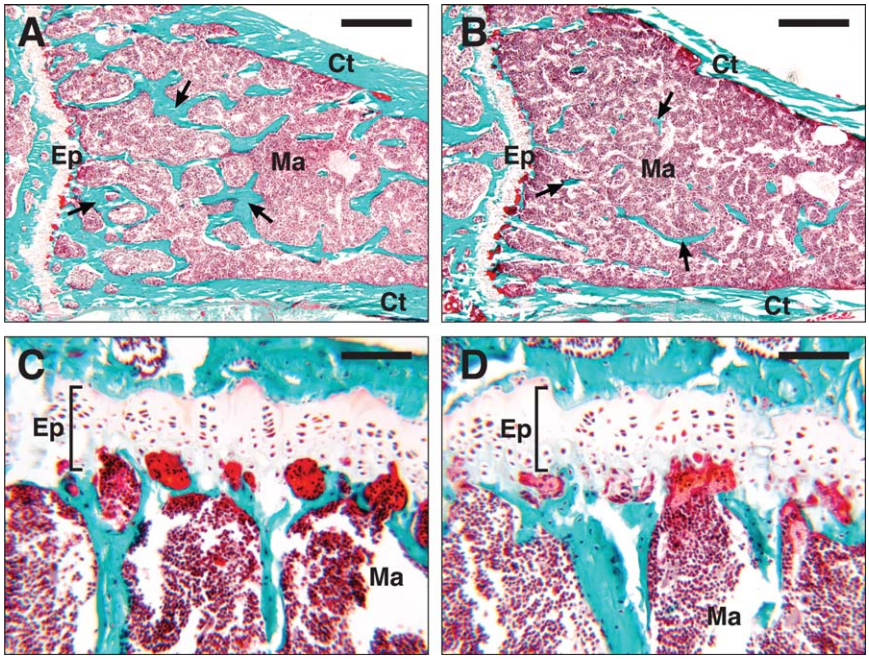

Fig. 1. Representative micrographs of the tibial metaphyses of **(A)** wild-type and **(B)** ICR/Mlac-*hydro* mice. Tissue sections (proximal tibiae) were processed for Goldner's trichrome staining. Mineralized matrix, erythrocytes, and cytoplasm were stained green, orange, and red, respectively. The numbers of metaphyseal trabeculae (arrows) in ICR/Mlac-*hydro* mice were markedly less than those in wild-type mice, resulting in expansion of the marrow space (Ma). Ep and Ct denote epiphyseal plate (also known as growth plate) and cortical envelope, respectively. Scale bars = 1000 μm. **C,D:** Magnified images of the proximal tibial growth plates of the wild-type mice and ICR/Mlac-*hydro* mice, respectively. Scale bars = 100 μm.

the tibial cortical envelope in each stained section was measured by ImageJ 1.46 (http://rsbweb.nih.gov/ij/index.html). Osteocyte lacunae that were not in the focal plane or had ill-defined borders were excluded from analysis (Charoenphandhu et al., 2012). The nomenclature, symbols, and units complied with the report of the American Society for Bone and Mineral Research Nomenclature Committee (Parfitt et al., 1987).

Determination of the Cortical Parameters and Moment of Inertia (MMI)

Cortical bone mineral density (Ct.BMD, g/mm^3), cortical periosteal perimeter (Ct.Pe.Pm, mm), cortical bone area (Ct.B.Ar, mm^2), and MMI values (mm^4) of *ex vivo* tibiae were analyzed by microcomputed tomography (μCT; model SkyScan 1178; voxel size of 85 μm^3; SkyScan, Kontich, Belgium), as described previously (Charoenphandhu et al., 2012). The equipment had X-ray tube voltage of 65 kV, current of 615 μA, and 0.5-mm aluminum filter. The scanning angular rotation was 180° with angular increment in 0.54°. The volume of interest (VOI) was between 1.43 and 1.86 mm distal to the proximal tibial growth plate (50 slides). Images were reconstructed and analyzed by a computer cluster running SkyScan CT-analyzer software package (version 1.11.10). MMI that represented the resistance to bending around *x*- or *y*-axis lying in the cross-sectional plane (MMIx and MMIy), and polar MMI were determined.

Statistical Analysis

Results are expressed as means ± standard error. The data were analyzed by unpaired Student's *t*-test (one-tailed) using GraphPad Prism 6.0 (GraphPad Software, San Diego, CA). The statistical significance was considered when $P < 0.05$.

RESULTS

As compared to the wild-type mice, the ICR/Mlac-*hydro* mice showed hyperphosphatemia, a sign of impaired kidney function, but had similar levels of BUN

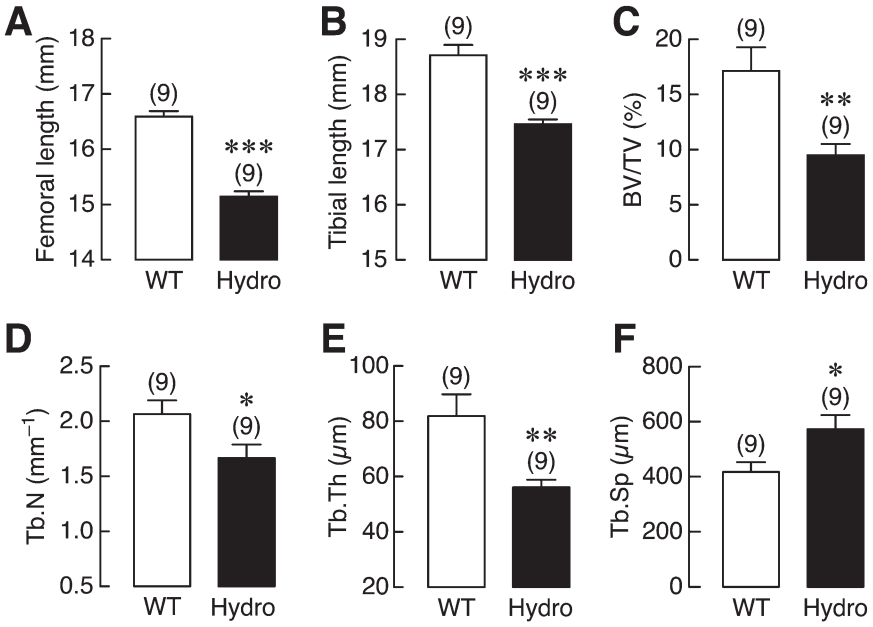

Fig. 2. **(A)** Femoral length, **(B)** tibial length, **(C)** trabecular bone volume (BV) normalized by tissue volume (TV), **(D)** trabecular number (Tb.N), **(E)** trabecular thickness (Tb.Th), and **(F)** trabecular separation (Tb.Sp) in the proximal tibial metaphyses of wild-type (WT), and ICR/Mlac-*hydro* (Hydro) mice. BV/TV, Tb.N, Tb.Th, and Tb.Sp were from Goldner's trichrome-stained sections as determined by bone histomorphometric analysis. Bone length was measured with a vernier caliper. Numbers of animals per group are noted in parentheses. $^{*}P < 0.05$, $^{**}P < 0.01$, $^{***}P < 0.001$ compared with WT.

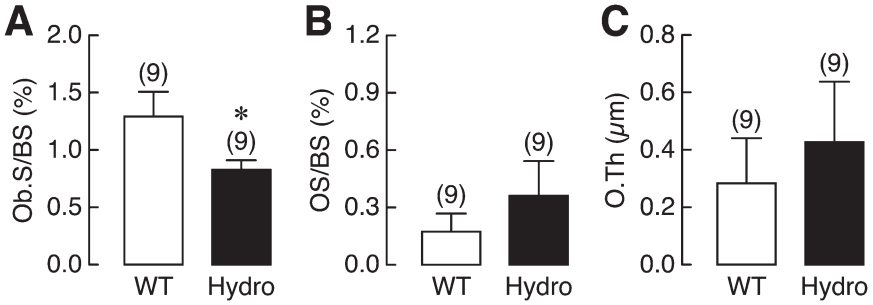

Fig. 3. **(A)** Osteoblast surface (Ob.S) normalized by bone surface (BS), **(B)** osteoid surface (OS) normalized by BS, and **(C)** osteoid thickness (O.Th) in the proximal tibial metaphyses of wild-type (WT) and ICR/Mlac-*hydro* (Hydro) mice. Ob.S/BS, OS/BS, and O.Th were from Goldner's trichrome-stained sections as determined by bone histomorphometric analysis. Numbers of animals per group are noted in parentheses. $^{*}P < 0.05$ compared with WT.

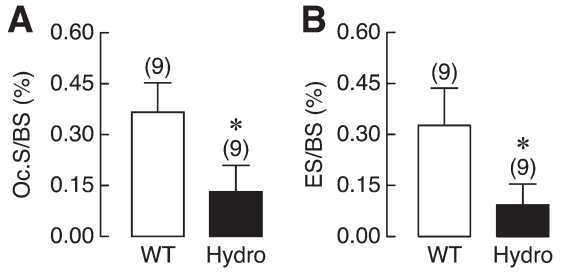

Fig. 4. **(A)** Osteoclast surface (Oc.S) normalized by bone surface (BS) and **(B)** eroded surface (ES) normalized by BS in the proximal tibial metaphyses of wild-type (WT) and ICR/Mlac-*hydro* (Hydro) mice. Oc.S/BS and ES/BS were from Goldner's trichrome-stained sections as determined by bone histomorphometric analysis. Numbers of animals per group are noted in parentheses. $^{*}P < 0.05$ compared with WT.

and creatinine (Table 1). Their 25-hydroxyvitamin D levels (64.94 ± 4.36 ng/mL, $n = 5$) were within the normal range of 40–80 ng/mL, whereas ionized calcium levels of mutant mice were lower than that of the wild-type mice (Table 1). These ICR/Mlac-*hydro* mice manifested impaired bone metabolism at both gross and microstructural levels as indicated by marked reductions in the femoral length, tibial length and calcified trabeculae in the proximal tibial metaphysis (green color in the Goldner's trichrome-stained sections), thereby resulting in a decreased trabecular bone volume and expansion of the marrow cavity as compared to the age-matched wild-type littermates (Figs. 1, 2). In addition, the ICR/Mlac-*hydro* mice exhibited decreases in trabecular number and trabecular thickness, whereas the trabecular separation was increased (Fig. 2). However, changes in the

growth plate appearance or cell morphology in each zone were not observed (Fig. 1).

Further histomorphometric analysis revealed suppression of bone formation in hydronephrotic mice as indicated by a decrease in the osteoblast surface without changes in osteoid surface ($P = 0.188$) or osteoid thickness ($P = 0.297$) (Fig. 3). A decrease in the osteoclast-mediated bone resorption was also evident as indicated by 64 and 72% reduction in the osteoclast surface and eroded surface, respectively, compared with the wild-type mice (Fig. 4). However, osteocyte lacunar area of the ICR/Mlac-*hydro* mice was similar to that of the wild-type mice ($P = 0.301$; Fig. 5). In addition, this μCT analysis suggested a decrease in bone strength in the ICR/Mlac-*hydro* mice as cortical bone mineral density, cortical periosteal perimeter, cortical bone area, and MMI values of the ICR/Mlac-*hydro* mice were lower than those of the wild-type littermates (Fig. 6).

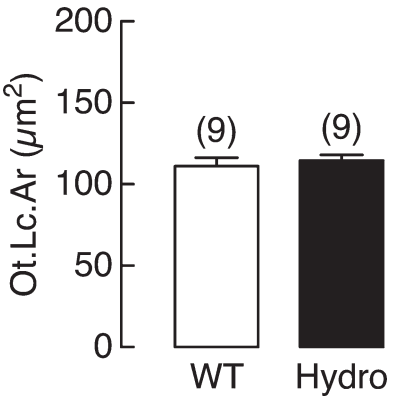

Fig. 5. Osteocyte lacunar area (Ot.Lc.Ar) in the tibial cortical envelope of wild-type (WT) and ICR/Mlac-*hydro* (Hydro) mice. Ot.Lc.Ar was obtained from Goldner's trichrome-stained tibial sections. Numbers of animals per group are noted in parentheses.

DISCUSSION

Alterations of bone microstructure are often observed in kidney diseases, especially in patients with diabetes mellitus, hypertension, or glomerulonephritis (Alpers, 2010). Although hydronephrosis is one of renal anomaly, which may or may not result in renal function impairment depending on the degree of renal tissue damage and duration of the disease, little is known regarding bone change associated with it. Our ICR/Mlac-*hydro* mice showed a marked loss of medullary and papillary tissue with renal tissue compression from trapped fluid (Kengkoom et al., 2012). However, this mouse strain did not develop full-blown chronic kidney disease as BUN and blood creatinine appeared normal. This bone histomorphometric analysis of hydronephrotic mice collectively suggested a low cellular activity of bone cells, that is, reductions in osteoblast and osteoclast surfaces (Figs. 3, 4), but normal mineralization as indicated by unaltered osteoid surface and osteoid thickness in both groups. Thus, hydronephrosis might be another important cause of bone defect. It has been known that aberrant bone metabolism in kidney diseases predisposes the animals to fracture due to weakened trabecular microstructure and delayed repair of microcracks in bone tissue (Coco and Rush, 2000). Nevertheless, as the underlying mutation in this mouse strain remains unknown, one cannot rule out the possibility that the

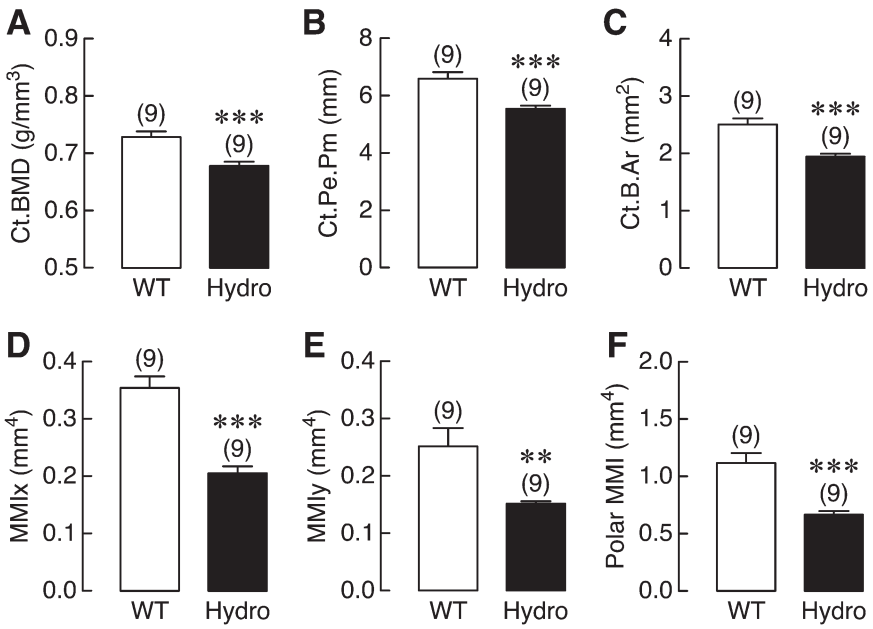

Fig. 6. **(A)** Cortical bone mineral density (Ct.BMD), **(B)** cortical periosteal perimeter (Ct.Pe.Pm), **(C)** cortical bone area (Ct.B.Ar), (**D** and **E**) moment of inertia (MMI) along the *x*- and *y*-axes, and **(F)** polar MMI in the tibiae of wild-type (WT) and ICR/Mlac-*hydro* (Hydro) mice. Numbers of animals per group are noted in parentheses. $^{**}P < 0.01$, $^{***}P < 0.001$ compared with WT.

mutation may directly impair functions of bone cells, leading to a phenotype of bone loss.

Interestingly, this histomorphometric data showed a reduction on osteoblast surfaces, which was suggestive of a reduction in tissue- and organ-level bone formation. Multiple factors are known to contribute to low bone formation, for example, an impaired phosphate metabolism, bone resistance to parathyroid hormone, abnormal $1,25(OH)_2D_3$ production, metabolic acidosis, high serum phosphate, elevated circulating cytokine levels [e.g., tumor necrosis factor (TNF)-α, interleukin (IL)-1, and IL-6] and decreased estrogen and testosterone levels (Andress, 2008). As 25-hydroxyvitamin D levels were within the normal range, impaired bone formation in the ICR/Mlac-*hydro* mice did not result from vitamin D deficiency, but inadequate renal conversion of 25-hydroxyvitamin D to $1,25(OH)_2D_3$ by 1α-hydroxylase could not be ruled out. Hyperphosphatemia might also contribute to a decreased osteoblast function, and could reduce 1α-hydroxylase activity (Weselling et al., 2008), leading to lower $1,25(OH)_2D_3$ and ionized calcium levels in ICR/Mlac-*hydro* mice. In addition, it was evident that high levels of proapoptotic factors, for example, TNF-α and IL-1, were associated with osteoblast apoptosis in chronic kidney disease (Tsuboi et al., 1999; Andress, 2008).

A decrease in bone resorption as indicated by reductions in the osteoclast surface and eroded surface was also observed in hydronephrotic mice. Although it was not clear what caused these reductions, it was possible that they were secondary to the hydronephrosis-induced metabolic disturbances, such as chronic metabolic acidosis (Chandar et al., 1996). Domrongkitchaiporn et al. (2001) demonstrated in patients with distal renal tubular acidosis (dRTA) that chronic metabolic acidosis suppressed both bone formation and bone resorption, thereby leading to low bone mass in the dRTA patients. Low osteoblast activity might also result in a decreased production of osteoblast-derived osteoclastogenic factors, such as receptor activator of nuclear factor κB ligand (RANKL), which, in turn, diminished osteoclastogenesis (Matsuo and Irie, 2008). Moreover, as the formation of active multinucleated osteoclasts requires the presence of $1,25(OH)_2D_3$ (Zaidi, 2007; Matsuo and Irie, 2008; Kogawa et al., 2010), the synthesis of which is mediated by the renal enzyme 1α-hydroxylase (Matsumoto et al., 1992), it is speculated that an impaired $1,25(OH)_2D_3$ production—as commonly found in chronic kidney disease patients—could contribute to low osteoclastogenesis in hydronephrotic mice (de Boer, 2008). On the other hand, the absence of change in osteocyte lacunar area suggested that osteocytic osteolysis did not contribute to bone loss in the ICR/Mlac-*hydro* mice.

Besides the presence of defective tibial microstructure, measurement of bone length revealed shorter femoral and tibial lengths of hydronephrotic mice. This suggested that hydronephrosis not only impaired trabecular bone turnover but also impaired growth plate function and longitudinal bone growth, despite no change in the histologic growth plate appearance (Fig. 1). Furthermore, decreases in cortical bone mineral density, cortical periosteal perimeter, cortical bone area, and MMI indicated a reduction in bone strength, particularly in the tibial diaphyses of ICR/Mlac-*hydro* mice. Chronic renal impairment in children and adolescents is usually associated with disorders of bone metabolism, which later impairs bone strength and finally reduces adult height (Wesseling et al., 2008). Thus, growth retardation is the most common clinical feature of chronic kidney disease in children (Sanchez, 2008; Wesseling et al., 2008). Metabolic acidosis and end organ resistance to growth hormone (GH) and insulin-like growth factor (IGF)-1 are major factors contributing to the growth failure (Wesseling et al., 2008). In addition, an increased production of IGF-binding proteins (IGFBP), for example, IGFBP-1 and -2, in individuals with renal impairment could decrease bioavailability of IGF-1 (Tönshoff et al., 1997; Wesseling et al., 2008). A recent investigation in uremic rats revealed that GH therapy following subtotal nephrectomy improved longitudinal bone growth by enhancing growth plate IGF-1 synthesis and chondrocyte proliferation (Barbosa et al., 2007).

In conclusion, ICR/Mlac-*hydro* mouse showed histologic features of low bone formation and resorption. These hydronephrotic mice also manifested an impaired longitudinal bone growth and a number of trabecular microstructural changes, such as an increase in trabecular separation and decreases in trabecular number and thickness, similar to that observed in chronic kidney disease. However, more investigation is required to reveal the hormonal profile as well as the cellular and molecular mechanisms of bone changes in hydronephrosis.

ACKNOWLEDGEMENTS

The authors thank Siwaporn Thobang and Natchayaporn Thonapan for technical assistance.

LITERATURE CITED

Alpers CE. 2010. The kidney. In: Kumar V, editor. Robbins and Cotran pathologic basis of disease. 8th ed. Philadelphia: Saunders–Elsevier. p 905–970.

Ampawong S, Klincomhum A, Likitsuntonwong W, Singha O, Ketjareon T, Panavechkijkul Y, Zaw KM, Kengkoom K. 2012. Expression of aquaporin-1, -2 and -4 in mice with a spontaneous mutation leading to hydronephrosis. J Comp Pathol 146:332–337.

Andress DL. 2008. Adynamic bone in patients with chronic kidney disease. Kidney Int 73:1345–1354.

Arnett T. 2003. Regulation of bone cell function by acid-base balance. Proc Nutr Soc 62:511–520.

Barbosa AP, Silva JD, Fonseca EC, Lopez PM, Fernandes MB, Balduino A, Duarte ME. 2007. Response of the growth plate of uremic rats to human growth hormone and corticosteroids. Braz J Med Biol Res 40:1101–1109.

Brandao-Burch A, Utting JC, Orriss IR, Arnett TR. 2005. Acidosis inhibits bone formation by osteoblasts in vitro by preventing mineralization. Calcif Tissue Int 77:167–174.

Chandar J, Abitbol C, Zilleruelo G, Gosalbez R, Montané B, Strauss J. 1996. Renal tubular abnormalities in infants with hydronephrosis. J Urol 155:660–663.

Charoenphandhu N, Suntornsaratoon P, Jongwattanapisan P, Wongdee K, Krishnamra N. 2012. Enhanced trabecular bone resorption and microstructural bone changes in rats after removal of the cecum. Am J Physiol Endocrinol Metab 303:E1069–E1075.

Coco M, Rush H. 2000. Increased incidence of hip fractures in dialysis patients with low serum parathyroid hormone. Am J Kidney Dis 36:1115–1121.

de Boer IH. 2008. Vitamin D and glucose metabolism in chronic kidney disease. Curr Opin Nephrol Hypertens 17:566–572.

Domrongkitchaiporn S, Pongsakul C, Stitchantrakul W, Sirikulchayanonta V, Ongphiphadhanakul B, Radinahamed P, Karnsombut P, Kunkitti N, Ruang-raksa C, Rajatanavin R. 2001. Bone mineral density and histology in distal renal tubular acidosis. Kidney Int 59:1086–1093.

Faje A, Klibanski A. 2012. Body composition and skeletal health: too heavy? too thin? Curr Osteoporos Rep 10:208–216.

Jongwattanapisan P, Suntornsaratoon P, Wongdee K, Dorkkam N, Krishnamra N, Charoenphandhu N. 2012. Impaired body calcium metabolism with low bone density and compensatory colonic calcium absorption in cecectomized rats. Am J Physiol Endocrinol Metab 302:E852–E863.

Kengkoom K, Zaw KM, Inpunkaew R, Angkhasirisap W, Thongsiri P, Ampawong S. 2012. Development of hydronephrosis inbred strain mouse, ICR/Mlac-*hydro*. J Anim Vet Adv 11:2054–2058.

Kogawa M, Findlay DM, Anderson PH, Ormsby R, Vincent C, Morris HA, Atkins GJ. 2010. Osteoclastic metabolism of 25(OH)-vitamin D_3: a potential mechanism for optimization of bone resorption. Endocrinology 151:4613–4625.

Matsumoto T, Yamato H, Okazaki R, Kumegawa M, Ogata E. 1992. Effect of 24,25-dihydroxyvitamin D_3 in osteoclasts. Proc Soc Exp Biol Med 200:161–164.

Matsuo K, Irie N. 2008. Osteoclast-osteoblast communication. Arch Biochem Biophys 473:201–209.

Parfitt AM, Drezner MK, Glorieux FH, Kanis JA, Malluche H, Meunier PJ, Ott SM, Recker RR. 1987. Bone histomorphometry: standardization of nomenclature, symbols, and units. Report of the ASBMR Histomorphometry Nomenclature Committee. J Bone Miner Res 2:595–610.

Sanchez CP. 2008. Mineral metabolism and bone abnormalities in children with chronic renal failure. Rev Endocr Metab Disord 9: 131–137.

Suntornsaratoon P, Wongdee K, Goswami S, Krishnamra N, Charoenphandhu N. 2010. Bone modeling in bromocriptine-treated pregnant and lactating rats: possible osteoregulatory role of prolactin in lactation. Am J Physiol Endocrinol Metab 299: E426–E436.

Thongchote K, Svasti S, Sa-ardrit M, Krishnamra N, Fucharoen S, Charoenphandhu N. 2011. Impaired bone formation and osteopenia in heterozygous $\beta^{IVSII-654}$ knockin thalassemic mice. Histochem Cell Biol 136:47–56.

Toiviainen-Salo S, Garel L, Grignon A, Dubois J, Rypens F, Boisvert J, Perreault G, Decarie JC, Filiatrault D, Lapierre C, Miron MC, Bechard N. 2004. Fetal hydronephrosis: is there hope for consensus? Pediatr Radiol 34:519–529.

Tönshoff B, Powell DR, Zhao D, Durham SK, Coleman ME, Domené HM, Blum WF, Baxter RC, Moore LC, Kaskel FJ. 1997. Decreased hepatic insulin-like growth factor (IGF)-I and increased IGF binding protein-1 and -2 gene expression in experimental uremia. Endocrinology 138:938–946.

Tsuboi M, Kawakami A, Nakashima T, Matsuoka N, Urayama S, Kawabe Y, Fujiyama K, Kiriyama T, Aoyagi T, Maeda K, Eguchi K. 1999. Tumor necrosis factor-α and interleukin-1β increase the Fas-mediated apoptosis of human osteoblasts. J Lab Clin Med 134:222–231.

van't Hof RJ, Clarkin CE, Armour KJ. 2003. Studies of local bone remodeling: the calvarial injection assay. In: Helfrich MH, Ralston SH, editors. Bone research protocols, 1st ed. New Jersey: Humana Press. p 345–351.

Wesseling K, Bakkaloglu S, Salusky I. 2008. Chronic kidney disease mineral and bone disorder in children. Pediatr Nephrol 23:195–207.

Zaidi M. 2007. Skeletal remodeling in health and disease. Nat Med 13:791–801.